HHS Public Access

Author manuscript

Lab Invest. Author manuscript; available in PMC 2016 May 01.

Published in final edited form as:

Lab Invest. 2015 November ; 95(11): 1305–1318. doi:10.1038/labinvest.2015.113.

Partial Denervation of Subbasal Axons Persists Following Debridement Wounds to the Mouse Cornea

Ahdeah Pajoohesh-Ganji[1], **Sonali Pal-Ghosh**[1], **Gauri Tadvalkar**[1], **Briana M. Kyne**[1,2], **Daniel R. Saban**[3], and **Mary Ann Stepp**[1,4,*]

[1]Department of Anatomy and Regenerative Biology, The George Washington University Medical School, Washington, DC 20037

[2]Physiology and Neuroscience Program, University of Maryland, College Park MD 20740

[3]Department of Ophthalmology, Duke Eye Center, Duke University, Durham, NC 27710

[4]Department of Ophthalmology, The George Washington University Medical School, Washington, DC 20037

Abstract

Although sensory reinnervation occurs after injury in the PNS, poor reinnervation in the elderly and those with diabetes often leads to pathology. Here we quantify subbasal axon density in the central and peripheral mouse cornea over time after three different types of injury. The mouse cornea is highly innervated with a dense array of subbasal nerves that form a spiral called the vortex at the corneal center or apex; these nerves are readily detected within flat mounted corneas. After anesthesia, corneal epithelial cells were removed using either a dulled blade or a rotating burr within an area demarcated centrally with a 1.5 mm trephine. A third wound type, superficial trephination, involved demarcating the area with the 1.5 mm trephine but not removing cells. By 7d after superficial trephination, subbasal axon density returns to control levels; by 28d the vortex reforms. Although axon density is similar to control 14d after dulled blade and rotating burr wounding, defects in axon morphology at the corneal apex remain. After 14d, axons retract from the center leaving the subbasal axon density reduced by 37.2% and 36.8% at 28d after dulled blade and rotating burr wounding, respectively, compared to control. Assessment of inflammation using flow cytometry shows that persistent inflammation is not a factor in the incomplete reinnervation. Expression of mRNAs encoding 22 regeneration associated genes (RAGs) involved in axon targeting assessed by QPCR reveals that netrin-1 and ephrin signaling are altered after wounding. Subpopulations of corneal epithelial basal cells at the corneal apex stop expressing ki67 as early as 7d after injury and by 14d and 28d after wounding, many of these basal cells undergo apoptosis and die. While subbasal axons are restored to their normal density and morphology after superficial trephination, subbasal axon recovery is partial after debridement wounds. The increase in corneal epithelial basal cell apoptosis at the apex observed at 14d after

*Author to whom correspondence should be addressed: Mary Ann Stepp, Ph.D., GWU Medical School, Dept. of Anatomy and Regenerative Biology, 2300 I St NW, Washington DC 20037, 1-202-994-0557.

corneal debridement may destabilize newly reinnervated subbasal axons and lead to their retraction towards the periphery.

Introduction

The cornea is one of the most highly innervated tissues in the body[1]. A dense ordered array of subbasal axons innervates the cornea from nerve cell bodies located primarily in the ophthalmic branch of the trigeminal ganglion. When severed surgically or damaged as a result of stroke or injury, the ocular surface rapidly develops pathology referred to as neurotrophic keratitis with epithelial erosions as symptoms[2–4].

The subbasal axons are unmyelinated and branch from larger axons located in the stroma[1]. A single stromal axon gives rise to numerous collateral subbasal axons; branches emerge from subbasal axons and project towards the apical surface. Most subbasal axons penetrate the epithelial basement membrane from the anterior stroma at the corneal periphery. They localize between the basal surface of the corneal epithelial cells and the basement membrane and run parallel to the ocular surface assuming a distinctive pinwheel pattern as they converge at the corneal apex[2]. The pattern formed by the subbasal axons is a Phi spiral, which arises frequently in nature and is seen in rat and, to a limited extent, human corneas[5,6]. The Phi spiral is shown in the unwounded mouse cornea in Figure 1 and will be referred to here as the vortex.

To generate a wound of a specific size, a dulled trephine is placed on the anesthetized ocular surface at the corneal center and rotated forming an impression crushing the epithelial cells and severing the subbasal axons at the trephine site. Superficial trephination partially denervates the central 1.5 mm of the cornea since subbasal axons that emerge from the stroma inside the 1.5 mm area are not severed. By contrast, rotating burr and dulled blade wounds eliminate all of the subbasal axons within the region defined by the trephine[7,8]; the rotating action of the burr partially removes the basement membrane and more cellular and axon debris compared to dulled blade[8]. Although dulled blade wounds to the mouse cornea close within 24 hours, recurrent epithelial erosions begin to develop two weeks after wounding[9]. While corneal clouding can be observed by 6–8 weeks after injury, corneas with recurring erosions are stable over time[10]. It is not known whether the subbasal axons will be able to re-form a vortex after dulled blade or rotating burr injury.

Unlike the central nervous system (CNS), the axons of the peripheral nervous system (PNS) regenerate well[11]. Within hours after PNS axonal injury, new growth cones develop and axons begin to elongate into wound sites[12]. The extension of a growth cone after injury involves activation of focal adhesion kinase and Src and is accompanied by changes in axonal microtubule assembly and membrane recycling[13,14]. PNS axons are stabilized within tissues by adhering to cells and to the matrix via adhesion molecules including β1-family integrins; regeneration requires integrins on axons and complimentary integrin ligands in the matrix to stabilize their adhesion and prevent retraction of newly extended axons towards the neuron soma[10,15].

In the unwounded cornea, epithelial basal cells adhere to the basement membrane primarily via hemidesmosomes that contain α6β4 integrin, and secondarily via α3β1 and αvβ5[16,17]. Because hemidesmosomes do not form between epithelial basal cells and axons, subbasal axons reduce corneal epithelial adhesion to the basement membrane. The sheer surface of the cornea further reduces the surface area available for adhesion. Together these anatomical features predispose the cornea to debridement injuries[18–20].

Regenerating subbasal axons encounter an extracellular matrix different from that in the unwounded cornea. Following superficial trephination, severed subbasal axons form growth cones that extend axons along the basement membrane. These growth cones navigate around hemidesmosomes and focal adhesions as they target the corneal apex. During reepithelialization, axons extend under migrating corneal epithelial cell sheets on substrates consisting of remnants of disrupted basement membrane and laminin expressed by migrating epithelial cells. MMP expression is upregulated during sheet movement and MMPs target both integrins and ECM molecules in the basement membrane for cleavage. Integrin ligand availability for corneal epithelial cell and axon adhesion changes as the basement membrane is resynthesized[9,10,21].

Regeneration associated genes (RAGs) can both enhance (Semaphorins, neuropilins, netrins) or repel (netrin-1, Repulsive guidance molecule (Rgm) – a and b, ephrins) axon guidance and targeting[22]. Alterations in the expression or function of RAGs by both corneal cells and trigeminal neurons likely play roles in regulating corneal reinnervation. mRNAs synthesized in neuron somas can be transported along axons towards growth cones and used to direct protein synthesis locally[23,24]. Cytokine release caused by inflammation also impacts the ability of both CNS and PNS axons to regenerate[22,25]. The factors mentioned above, individually or collectively, likely impact subbasal axon regeneration after corneal injury. The fact that the density of subbasal sensory axons is greater in the cornea than in any other tissue, the strong base of knowledge obtained over the years about corneal wound healing, and the improved methods for acquiring confocal and 3D images, make the mouse cornea an ideal model to study axonal reinnervation in the PNS.

Here we quantify axon density as a function of time during axon regeneration after three different types of corneal injury, perform flow cytometry to quantify inflammation, assess mRNA expression of numerous RAGs involved in axon guidance by QPCR, and evaluate the involvement of corneal epithelial cell apoptosis in defective denervation. To our knowledge, this is the first quantitative assessment of long-term reinnervation of the subbasal axons in the mouse cornea.

Materials and Methods

Corneal wounding

All studies performed comply with the George Washington University Medical Center Institutional Animal Care and Use Committee guidelines and with the ARVO Statement for the Use of Animals in Vision Research. Male BALB/c mice (NCI, Frederick, MD, USA), 8 weeks old, were used for all of the experiments described. Mice were anesthetized with ketamine/xylazine and a topical anesthetic applied to their ocular surface. A 1.5-mm

trephine was used to demarcate the wound area. For the superficial trephination studies, no further treatment was performed. However, for debridement, epithelial tissues within the trephine area were removed using either a dulled blade or a rotating burr (AlgerbrushII; Ambler Surgical, Exton, PA, USA) with a 0.5-mm burr tip. After wounding, erythromycin ophthalmic ointment was applied to the injured cornea and allowed to heal for different times after which they were euthanized. For immunofluorescence studies tissues were fixed immediately (1x PBS, 1% formaldehyde, 2mM Mgcl2, 5mM EGTA, 0.02% NP-40, Water) for 1 hr and 15 min at 4°C, followed by 2 washes for 10 min each in 1x PBS with 0.02%NP40 at room temperature. Tissues were placed in 4:1 Methanol: DMSO at −20°C for 2 hours and then to 100% Methanol for long-term storage. Vybrant Apoptosis Assay Kit #5, Hoechst 33342/Propidium Iodide (Life technologies; #V13244) was used for apoptosis study. For Hoechst/PI studies, corneas were incubated with 1:500 of Hoechst and PI in 1XPBS at 4°C for 30 minutes. The eyes were then rinsed with 1x PBS and fixed as mentioned above.

Microscopy

For Sholl analysis, images were acquired using the Zeiss Cell Observer Z1 spinning disk confocal microscope (Carl Zeiss, Inc., Thornwood, NY, USA), equipped with ASI MS-2000 (Applied Scientific Instrumentation, Eugene, OR, USA) scanning stage with z-galvo motor, and Yokogawa CSU-X1 spinning disk. A multi-immersion 25-x/0.8 objective lens, LCI Plan-Neofluor, was used for imaging, with oil immersion. Evolve Delta (Photometrics, Tucson, AZ, USA) 512 × 512 EM-CCD camera was used as detector (80-msec exposure time). A diode laser emitting at 488 nm was used for excitation (54% power). Zen Blue software (Carl Zeiss, Inc.) was used to acquire the images, fuse the adjacent tiles, and produce maximum intensity projections. The adjacent image tiles were captured with overlap to ensure proper tiling. All images were acquired using the same intensity settings. Samples for Sholl analysis were taken from regions indicated by white circles from each eye as shown in supplemental Figure 1. Circles numbered 1–4 were averaged as peripheral and 5–7 were averaged as central samples.

Confocal microscopy was performed at the Center for Microscopy and Image Analysis (CMIA) at the George Washington University Medical Center. A confocal laser-scanning microscope (Zeiss 710) equipped with a krypton-argon laser was used to image the localization of Alexa Fluor 488 (488 nm laser line excitation; 522/35 emission filter), and Alexa Fluor 594 (568 nm excitation; 605/32 emission filter). Optical sections (z=0.5 μm or 1 μm) were acquired sequentially with a 10x, 20x, 40x or 63x objective lens. The 3D images presented were generated using Volocity software (Version 5.0, Perkin Elmer). A Nikon fluorescent microscope using 10x and 40x objectives and equipped with a SPOT RT3 camera running SPOT software 5.0.27 were used to visualize the Hoechst/PI staining.

Antibodies

Corneas were stained with the following antibodies: rabbit monoclonal against Ki67 (Abcam, #ab16667), β III tubulin (Covance; #MMS-435P-100), and Phospho-Histone H2A.X (Ser139) (20E3) rabbit monoclonal antibody (Cell signaling; #9718S). Appropriate secondary DyLite 488 or 594 antibodies from Jackson ImmunoResearch were used for

immunolabeling. Corneas were stained with DAPI (Thermo fisher; #46190) before flat mounting to reveal nuclei. To achieve the best flattening, the corneas were placed epithelial side-up with mounting media (Fluoromount G: Electron Microscopy Sciences; #17984-25) and coverslipped.

QPCR

1.5mm wound were made on the mouse cornea using dulled blade and rotating burr. Mice were sacrificed 4d, 7d, 14d, and 28d after wounding. Eyes were then enucleated and 2mm corneal buttons free of debris were dissected from the central cornea and frozen in liquid nitrogen individually. 12 corneas were used for the each time point. RNA was extracted from each corneal button using Arcturus Picopure RNA isolation kit (Applied Biosystems; #12204-01) according to the manufacturer's instructions. QPCR was performed using a Bio-Rad CFX384 Real-Time PCR detection system. The primers used are indicated in Supplemental Table 1. The abbreviations for each mRNA studied in Figure 5 and Supplemental Figure 2 were obtained from the Mouse Genome Informatics web site maintained by Jackson Labs [http://www.informatics.jax.org/marker]. Non-detects[26] and outliers [http://graphpad.com/quickcalcs/grubbs2/] for each of the variables assessed are indicated in Supplemental Table 2.

Flow Cytometry

For flow cytometry studies, dulled blade and rotating burr wounded corneas were obtained at the indicated times after wounding. Corneal buttons from both control and wounded mice were carefully dissected making sure to leave a minimal and uniform limbal rim. The corneal buttons were placed in ice-cold, serum-free media overnight. The number of corneas used per assay was 6–8 per variable and experiments were repeated a minimum of four times. The following day, corneas were digested with collagenase and released cells used for determination of immune cell subtypes as described previously[27]. The number of leukocytes present in the wounded corneas was compared with those present in naïve corneas and data were expressed as % CD45+ cells.

Statistical analyses

Quantitative data are presented as mean±standard error of the mean. All data were analyzed using Students t-test or one-way ANOVA. All statistical tests were performed using the GraphPad Prism Program, Version 6 for Windows (GraphPad Software, Inc. San Diego, CA). A p value<0.05 was considered statistically significant.

Results

Stable subbasal axon vortex reformation occurs after trephination but not after dulled blade and rotating burr wounding

When a single 1.5 mm debridement wound is made to the mouse cornea using a dulled blade, 80% of the corneas spontaneously develop recurrent erosions by 28d after wounding[9]. To determine whether defective subbasal nerve reinnervation contributes to erosion formation, here we assess reinnervation of the corneal subbasal axons as a function of time after dulled blade and rotating burr wounds which show a significantly lower frequency

(20%) of spontaneous erosion formation[9]. To differentiate between reinnervation after severing subbasal axons and removing epithelial cells from reinnervation after severing axons alone, we also evaluate corneas after superficial trephination with a 1.5 mm trephine. The trephination only wound model we employ denervates subbasal nerves exclusively unlike studies using a sharp trephine that denervate both anterior stromal and subbasal nerves[28].

Representative images showing the subbasal axons stained with βIII tubulin for an unwounded cornea and corneas at 1d, 2d, 3d, 4d, 7d, 14d, and 28d after wounding for each of the three wound types are presented in Figure 1. For each variable assessed, a montage was generated using spinning disk confocal imaging showing the area at the corneal center where the trephine was placed. A vortex is present in all of the unwounded corneas at the apex, which is slightly off center and shifted inferonasally[2]. When corneas are assessed minutes after dulled blade and rotating burr wounding, subbasal axons within the wound site are all eliminated[9].

To quantify differences in axon density over time after wounding, Sholl analysis was performed as described in the Methods section and Supplemental Figure 1; axon density was assessed at the periphery (defined as outside where the trephine was placed) and at the center within the trephine site of no fewer than 5 corneas per time point. The center axon densities are averages of three independent sites; typically, the center-most area has the lowest axon density but differences between corneas of individual mice contribute variability. Despite its quantitative value, axon density alone cannot determine whether stable corneal reinnervation takes place; image analysis is also needed to assess subbasal axon morphology and vortex reformation. Sholl data are presented in Figure 2 normalized by comparison to the axon density seen in the center and periphery of unwounded control corneas at 1, 2, 3, 4, 7, 14, and 28 days after wounding.

Axon density is significantly reduced for all three wound types compared to unwounded corneas at peripheral sites at 1d and 2d. Axon density in the periphery recovers to control levels for all three wound types by 14d. Recovery of axon density in the periphery is maintained through 28d.

Between 1d-4d after trephination, central axon density increases at each time point but remains significantly lower than control; by 7d, axon density is similar to control. However, the morphology of the subbasal axons in the majority of trephined corneas does not return to that of unwounded corneas with a well formed vortex until day 28 (Figure 1). Therefore, partial denervation of subbasal axons by superficial trephination permits complete reinnervation with reestablishment of the vortex 28d after wounding.

After both dulled blade and rotating burr wounding, axon density at the center remains significantly below control for 7d after wounding. At 14d, sites persist at the corneal apex after dulled blade and rotating burr wounding that lack axons (Figure 1); yet, axon density assessed by Sholl analysis within the center recovers to control levels (Figure 2). However, recovery is not maintained and, by 28d, axon density is once again lower centrally compared to unwounded control. Despite the fact that rotating burr wounded corneas develop erosions

less frequently than dulled blade wounded corneas[9], rotating burr and dulled blade wounded corneas show similar kinetics of axon recovery through 28d after wounding.

Subpopulations of corneal epithelial cells in the central cornea stop expressing ki67 14d after wounding

We next assessed the integrity of the ocular surface at 4d, 14d, and 28d after rotating burr wounding using confocal imaging and DAPI staining. We visualized subbasal axons using an antibody against βIII tubulin and assessed whether cells were actively moving through the cell cycle using an antibody against ki67 (Figure 3). As indicated by DAPI staining, 4d after wounding, the epithelium is intact. Numerous ki67+ cells are present at the corneal center at regions where subbasal axons are absent indicating that these cells are actively cycling.

By 14d, DAPI-staining reveals that the corneal epithelium remains intact although subtle irregularities evident as wrinkles and small gaps where cells are missing are seen (arrows); groups of cells not expressing ki67 (ki67–) are observed centrally that largely coincide with areas that lack subbasal axons. At 28d, ki67– cells at the center persist within denervated sites as do surface irregularities (arrowheads). Some corneas have sites showing increased DAPI staining suggestive of increased numbers of cell layers surrounding openings suggestive of early events in erosion formation (asterisk).

mRNA expression of *Ntn1* is reduced whereas *Efna5* is elevated 28d after dulled blade wounding

The analysis of mRNA expression for 22 RAGs in central corneal buttons was assessed by QPCR in control corneas and at 4d, 7d, 14d, and 28d after wounding; the identities of the RAGs assessed and their primers are shown in Supplemental Table 1. Because no differences in axon density are seen between dulled blade and rotating burr wounding over time by Sholl analysis (Figure 2), control and dulled blade wounded corneas are used. Presented in Figure 4A are data normalized relative to control for uncoordinated 5B (*Unc5B*), deleted in colorectal cancer (*Dcc*), neogenin-1 (*Neo1*), netrin-1 (*Ntn1*), repulsive guidance molecule a (*Rgma*), and *Rgmb*. Although a significant decrease in *Ntn1* levels relative to control and 7d is seen at 28d, mRNA for three netrin receptors (*Unc5B, Dcc*, and *Neo1*) is not altered at 28d. Although *Rgma* expression decreases at 14d and 28d after wounding compared to 4d and 7d, *Rgma* levels are similar to control at all time points assessed and no changes are seen in *Rgmb* expression.

Eph:ephrin signaling can regulate both axon guidance[2] and withdrawal of epithelial cells from the cell cycle and terminal differentiation[29]. When corneas are assessed for expression of *Efna4*, *Efna5, and Efnb1*, *Efna5* expression increases at each time point after wounding and becomes significantly elevated by 14d and 28d after wounding compared to control (Figure 4B). While expression of *Efna4* is increased at d14 compared to d4, compared to control, levels of both *Efna4* and *Efnb1* are not altered after injury.

We next looked at *Ngf, Ntf3*, *Ntrk2*, *Vegfa*, *and Vegfb* (Supplemental Figure 2). Differences are not seen between 14d and 28d when subbasal nerves retract. We also assessed

expression of several semaphorins (*Sema3a, Sema3f, Sema4d, Sema7a*), *Nrp1, Slit2, Robo2, and Sprr1a* (Supplemental Figure 2). Although there is a significant increase in *Sema4d* at 7d after wounding compared to 4d and control, no other significant differences are observed at 14d and 28d relative to control for the other seven mRNAs assessed.

More monocytes are recruited early after dulled blade wounding but inflammation does not persist

Persistent inflammation could lead to reinnervation defects after rotating burr and dulled blade wounds. Flow cytometry analyses were performed in control and corneas 0.75 (18 hr), 3, 7, 14, or 28d after wounding to determine whether alterations in leukocyte recruitment or retention are seen after rotating burr or dulled blade wounds. Results are presented in Figure 5A–C. At 18 hr after wounding, during active reepithelialization, significantly more PMNs (Ly6C+/Ly6G-hi) are present in both rotating burr and dulled blade wounds compared to control; no significant differences are seen between wound types. Between 3d-14d after wounding, the number of PMNs present after both wound types is similar to the number seen in unwounded corneas. At 28d, more PMNs are present in the rotating burr compared to dulled blade wounded and control corneas.

While monocytes (Ly6C-hi/Ly6G-lo) increase after both wound types, only after dulled blade wounds were the differences significant at 18hr and 3d after wounding compared to control. After 3d, the number of monocytes returned to control levels and remain low through 28d. Macrophage (Ly6C-lo/F4/80-hi) numbers were also assessed as a function of time after injury. Compared to control, there are no significant differences in the % CD45+ cells that are macrophages at time points after 18hr or between wound types at other time points.

Although the immune responses to dulled blade and rotating burr wounds were similar, differences were seen with respect to monocytes which were elevated after dulled blade wounds at 18hr and 3d. By 7d and 14d after both dulled blade and rotating burr wounds, the number of PMNs, monocytes, and macrophages are similar to those found in unwounded control. Persistent inflammation is not responsible for the incomplete reinnervation of the cornea after dulled blade and rotating burr wounds.

Corneal epithelial cell apoptosis and cell death are observed after rotating burr and dulled blade wounds

The absence of ki67 expression within a subpopulation of corneal epithelial cells lacking subbasal axons 14d and 28d after wounding (Figure 3) suggests that cells have entered the G0 phase of the cell cycle or that they are undergoing apoptosis. To investigate further, flat mounted corneas were stained to show the expression of γH2AX at 7, 14, and 28d after dulled blade wounding (Figure 6A). γH2AX is a histone family member expressed constitutively at a low level during cell cycle progression (γH2AXlo); when cells exit the cell cycle and enter G0, γH2AX expression ceases (γH2AX–). When double stranded DNA strand breaks are detected, cells dramatically up-regulate γH2AX expression (γH2AXbr)[30]. In addition to γH2AX, we also stained corneas with DAPI, and βIII tubulin.

At time points before 7d, γH2AXlo cells are uniformly distributed across the ocular surface (data not shown). DAPI staining at 7d is uniform and the epithelial sheet is intact. Clusters of epithelial cells at the corneal center are γH2AX– beginning at 7d and these sites persist at 14d and 28d. The marginal zones separating the γH2AXlo and the γH2AX–corneal epithelial cells do not correspond precisely, but overlap with sites where subbasal axons terminate.

At 14d and 28d, numerous corneal epithelial cells are γH2AXbr indicating the presence of double stranded DNA breaks characteristic of apoptotic cells (Figure 6A). High resolution confocal 3D imaging was performed to determine whether apoptotic cells were present in the basal or more apical cell layers (Figure 6B). Data show that the majority of γH2AXbr cells are in the basal cell layer. Although the data in Figures 6A and B are from corneas wounded by the dulled blade; corneas wounded with the rotating burr also develop γH2AX– patches near erosion sites and γH2AXbr cells are seen but not until 28d after wounding (data not shown).

To determine whether apoptotic cells were dying, corneas were also stained with Hoechst and PI prior to fixation (Figure 6C). Imaging PI and Hoechst stained flat mounted corneas reveals clusters of corneal epithelial cells near the center that are Hoechst-br, indicating an accelerated rate of corneal epithelial cell apoptosis. Some of the Hoechst-br cells are PI positive indicating that they are dead.

Discussion

Only corneas wounded by trephination reform a vortex

Our studies quantify reinnervation of the subbasal axons after three different types of injury. Many different methods could have been selected to quantitate reinnervation in the mouse cornea. Sholl analysis was used to allow us to focus on the overall numbers of subbasal axons present rather than their diameter and tortuosity. The density of axons remaining in the center of the wound (defined as the 1.5 mm area originally demarcated by the trephine) 1d after trephination is 46% of those in control. The density of subbasal axons in the center increases from 1d to 7d when the numbers are equal to those seen in control. While the density of axons indicates reinnervation by 7d, the vortex does not assume its typical morphology until 28d after wounding. An in vivo confocal imaging study of reinnervation of the mouse cornea after a smaller diameter (1.2 mm) but deeper trephination that severs anterior stromal and subbasal nerves showed that even 8 weeks after trephination, axon density remained significantly lower (73%–78%) than control[31]. While our study indicates that subbasal axons recover well after superficial trephination injuries, deeper trephination injuries severing anterior stromal nerves result in chronic denervation.

Reinnervation of subbasal axons is stalled 14d after 1.5 mm rotating burr and dulled blade wounding

Differences in axon density between dulled blade and rotating burr over time were not significant relative to one another. Axon density after both wound types was significantly lower than control throughout the first week after wounding. By 14d after wounding it

increases to control levels followed by a reduction to 61%–62% of the control by 28d. Although axon density was 100% at 14d, axon morphology was not restored; sites lacking axons remained adjacent to sites with numerous axons and the vortex was missing. Reductions in subbasal axon density are observed after corneal infections, PRK, LASIK, and in glaucoma patients[32–36]. In one study of glaucoma patients, a 21% reduction in subbasal axons did not impact corneal sensitivity assessed using Cochet-Bonnet esthesiometry[34]. A reduction in subbasal axon density does not always correlate with pathology of the ocular surface[37,38]. We did not perform Cochet-Bonnet esthesiometry after corneal wounding, so we do not know whether mouse corneas have defects in corneal sensitivity.

Altered expression of *Ntn1* and *Efna5* are seen 28d after corneal debridement wounding

Netrins (Ntns) are the mammalian homologs of UNC6, an ECM protein containing laminin motifs first identified in C elegans[39]. In axon guidance assays, Ntn1 bound to heparan sulfate coated beads attracts or repels axons depending on the receptors axons express[28,35]. Receptors for Ntn1 include several integrins, Dcc, Unc5B, and Neo1. Dcc, Unc5B, and Neo1 function as dependence receptors[39].

The 2 mm corneal buttons used in this study for QPCR contain mRNA from resident and recruited corneal cells (epithelial, stromal cells including leukocytes, and endothelial cells) and axons. Although some neuronal mRNAs are transported from the soma along axons and used to direct protein synthesis locally[40,41], the majority of the mRNA isolated from corneal buttons is derived from corneal epithelial cells which are present in a continuous sheet containing multiple layers of cells.

Expression of Ntn1 and its receptors is not restricted to neurons. Studies in the rat cornea show that Ntn1 and Unc5B proteins are expressed by corneal epithelial and to a lesser extent stromal cells[42]. In contrast to our data, the rat corneal studies show no mRNA expression in corneal buttons for *Dcc* and *Neo1*. Differences between the two studies could be due to differences between mouse and rat corneas or between the sensitivity of the methods used for RNA quantification.

Compared to control, *Ntn1* expression is decreased in corneal buttons taken from dulled blade wounded corneas but no significant changes are seen in expression of *Dcc*, *Unc5B*, or *Neo1* at 28d. *Unc5B* levels decrease at 4d but recover at 7d and 14d before dropping again at 28d. The decrease at 28d is significant relative to 7d but not compared to control. When *Ntn1* levels first begin to decrease relative to control at 14d after wounding, axon density has recovered to similar levels seen in control. Although the exact role played by Ntn1 signaling in the cornea is not known, studies in the chemically injured rat cornea implicate Ntn1 and Unc5B in stabilizing the ocular surface and reducing inflammation[42]. If Ntn1 produced in the cornea stabilizes epithelial cell and axon adhesion, reduced expression of Ntn1 could contribute to both axon retraction and erosion formation.

In general, activation of Eph signaling mediates axon repulsion[43] and also stimulates apoptosis and terminal differentiation in epidermal keratinocytes[29]. Skin wound healing studies in vivo show that neonatal sensory axon innervation is inhibited by several different ephrins. Ephrin-a (Efna) can induce growth cone collapse in cultured dorsal root ganglion

cells[43]. Treating epidermal keratinocytes with Efna4 and Efna5 *reduces* cell migration and integrin expression and *induces* expression of terminal differentiation markers[44]. Although studies looking at Eph-ephrin receptor distribution in the rat and human cornea[23,45] have yielded conflicting results regarding the numbers of distinct receptors and ligands expressed, Efna5 is present in the mammalian cornea.

The levels of *Efna5* increase at all the time points assessed after wounding; the increase is significant relative to control at 14d and 28d. Because axon density is similar to control at 14d when the increase in *Efna5* becomes significant, it is unlikely that Efna5 signaling impedes subbasal axon reinnervation. Elevated expression of Efna5 begins 7d after wounding. It could induce apoptosis in corneal epithelial basal cells resulting in reduced ki67 and γH2AX expression. As basal cells undergo apoptosis, their adhesion to the basement membrane and to subbasal axons is reduced. Depriving reinnervating subbasal axons of adhesion to basal cells at the corneal center over time would destabilize them leading to their retraction towards the corneal periphery.

Subpopulations of corneal epithelial cells over sites lacking subbasal axons withdraw from the cell cycle as early as 7d after wounding and begin to undergo apoptosis by 14d

As early as 7d after dulled blade wounding, clusters of epithelial cells at the corneal center stop expressing γH2AX. Sholl analysis shows that axon density at the corneal center 7d after dulled blade and rotating burr wounding is similar to that seen at 4d after wounding before groups of ki67– epithelial cells develop. Thus, reduced innervation at the corneal center alone does not appear to cause withdrawal of these corneal epithelial cells from the cell cycle. By 14d and 28d after wounding, some epithelial basal cells dramatically increase γH2AX expression and are apoptotic. PI staining shows dead cells among apoptotic cells. Another study showed increased TUNEL staining and decreased ki67 expression in the mouse cornea 7d after thermal ablation of the trigeminal ganglion[4]. The timing of the events studied in detail here indicate that while the local environment at the basement membrane zone at the corneal apex at 14d is permissive for reinnervation after dulled blade and rotating burr wounding, the apex microenvironment does not maintain adhesion of subbasal axons leading to their retraction.

Axon stalling and retraction: is corneal epithelial cell apoptosis involved?

Subbasal axons are embedded within a highly polarized microenvironment: their apical surface associates with the basal surfaces of corneal epithelial basal cells and their basal surface associates with ECM proteins in the basement membrane. The subbasal axon growth cones that extended towards the corneal center at 14d are maintained within the tissue by integrins and other adhesion proteins[10,15]. Increased numbers of epithelial basal cells at the center of the cornea undergoing apoptosis at 14d would destabilize the apical surface of the subbasal axons that lie beneath them.

Although the basement membrane was left intact after dulled blade wounding, migrating epithelial cells and immune cells degrade it during reepithelialization[17]; it takes between 2–3 weeks for the basement membrane to be reassembled[17]. The basal surfaces of reinnervated

subbasal axons 14d after wounding are adhering to a basement membrane that is partially reassembled[17].

Subbasal axon adhesion is therefore destabilized both apically and basally at the corneal center at 14d; further axon extension stalls and the vortex fails to reform. By 28d, enough subbasal axons have retracted to peripheral sites to significantly reduce axon density at the corneal center.

The mouse cornea is an excellent model to study the events that occur during regeneration of unmyelinated sensory axons. While all of the possible causes of subbasal axon instability after debridement wounds are not known, we show here that 1) persistent inflammation is not involved, 2) expression of *Ntn1* is reduced at 28d after wounding and expression of *Efna5* is increased 14d and 28d after wounding, 3) foci of corneal epithelial basal cells at the apex begin to withdraw from the cell cycle 7d after wounding and terminally differentiate in increased numbers beginning 14d and continuing through 28d after wounding. Sholl analysis shows axon density to be similar to control when corneal epithelial apoptosis is observed 14d after wounding. Corneal epithelial cell apoptosis appears to destabilize axon adhesion and induce retraction of subbasal axons between 14 and 28d after wounding.

Supplementary Material

Refer to Web version on PubMed Central for supplementary material.

Acknowledgments

We would like to thank Dr. Anastas Popratiloff, the director of center for microscopy and image analysis (CMIA) at the George Washington University, for his help with confocal microscopy. We acknowledge and appreciate the valuable advice of Drs. Beverly Oakley, Thomas Maynard, and Christophe Cataisson on QPCR data analysis. We further would like to thank Drs. Sue Menko and Janice Walker for numerous helpful discussions as this study progressed.

This work was funded by NIH grants EY08512, EY021784, and EY023106

Abbreviations

CNS	central nervous system
Dcc	deleted in colorectal cancer
PNS	peripheral nervous system
PBS	phosphate buffered saline
RAGs	Regeneration associated genes
UNC5B	uncoordinated 5B
Efna	ephrinA
Efnb	EphrinB
Ntrk2	TrkB neurotrophin receptor
Ntn1	netrin-1

Nrp1	neuropilin-1
Rgma	repulsive guidance molecule A
Rgmb	repulsive guidance molecule B
Ntf3	neurotrophic factor-3

References

1. Muller LJ, Marfurt CF, Kruse F, Tervo TM. Corneal nerves: structure, contents and function. Exp Eye Res. 2003; 76:521–42. [PubMed: 12697417]
2. Shaheen BS, Bakir M, Jain S. Corneal nerves in health and disease. Surv Ophthalmol. 2014; 59:263–85. [PubMed: 24461367]
3. Ueno H, et al. Dependence of corneal stem/progenitor cells on ocular surface innervation. Invest Ophthalmol Vis Sci. 2012; 53:867–72. [PubMed: 22232434]
4. Ferrari G, et al. A novel mouse model for neurotrophic keratopathy: trigeminal nerve stereotactic electrolysis through the brain. Invest Ophthalmol Vis Sci. 2011; 52:2532–9. [PubMed: 21071731]
5. Patel DV, McGhee CN. Mapping of the normal human corneal sub-Basal nerve plexus by in vivo laser scanning confocal microscopy. Invest Ophthalmol Vis Sci. 2005; 46:4485–8. [PubMed: 16303938]
6. Iannaccone S, et al. Three dimensional visualization and fractal analysis of mosaic patches in rat chimeras: cell assortment in liver, adrenal cortex and cornea. PLoS One. 2012; 7:e31609. [PubMed: 22347498]
7. Li Z, Burns AR, Rumbaut RE, Smith CW. gamma delta T cells are necessary for platelet and neutrophil accumulation in limbal vessels and efficient epithelial repair after corneal abrasion. Am J Pathol. 2007; 171:838–45. [PubMed: 17675580]
8. Pal-Ghosh S, et al. Cytokine deposition alters leukocyte morphology and initial recruitment of monocytes and gammadeltaT cells after corneal injury. Invest Ophthalmol Vis Sci. 2014; 55:2757–65. [PubMed: 24677104]
9. Pal-Ghosh S, Tadvalkar G, Jurjus RA, Zieske JD, Stepp MA. BALB/c and C57BL6 mouse strains vary in their ability to heal corneal epithelial debridement wounds. Exp Eye Res. 2008; 87:478–86. [PubMed: 18809399]
10. Pal-Ghosh S, et al. MMP9 cleavage of the beta4 integrin ectodomain leads to recurrent epithelial erosions in mice. J Cell Sci. 2011; 124:2666–75. [PubMed: 21750188]
11. DeFrancesco-Lisowitz A, Lindborg JA, Niemi JP, Zigmond RE. The neuroimmunology of degeneration and regeneration in the peripheral nervous system. Neuroscience. 2014
12. Siemionow M, Brzezicki G. Chapter 8: Current techniques and concepts in peripheral nerve repair. Int Rev Neurobiol. 2009; 87:141–72. [PubMed: 19682637]
13. Chen X, Gallar J, Belmonte C. Reduction by antiinflammatory drugs of the response of corneal sensory nerve fibers to chemical irritation. Invest Ophthalmol Vis Sci. 1997; 38:1944–53. [PubMed: 9331258]
14. Eva R, et al. Rab11 and its effector Rab coupling protein contribute to the trafficking of beta 1 integrins during axon growth in adult dorsal root ganglion neurons and PC12 cells. J Neurosci. 2010; 30:11654–69. [PubMed: 20810886]
15. Eva R, Fawcett J. Integrin signalling and traffic during axon growth and regeneration. Curr Opin Neurobiol. 2014; 27:179–85. [PubMed: 24793179]
16. Stepp MA, Spurr-Michaud S, Tisdale A, Elwell J, Gipson IK. Alpha 6 beta 4 integrin heterodimer is a component of hemidesmosomes. Proc Natl Acad Sci U S A. 1990; 87:8970–4. [PubMed: 2247472]
17. Stepp MA, et al. Wounding the cornea to learn how it heals. Exp Eye Res. 2014; 121:178–93. [PubMed: 24607489]

18. Watson SL, Lee MH, Barker NH. Interventions for recurrent corneal erosions. Cochrane Database Syst Rev. 2012; 9:CD001861. [PubMed: 22972054]
19. Laibson PR. Resistant herpes simplex keratitis. Clin Experiment Ophthalmol. 2010; 38:227–8. [PubMed: 20447115]
20. Ramamurthi S, Rahman MQ, Dutton GN, Ramaesh K. Pathogenesis, clinical features and management of recurrent corneal erosions. Eye (Lond). 2006; 20:635–44. [PubMed: 16021185]
21. Pal-Ghosh S, Pajoohesh-Ganji A, Tadvalkar G, Stepp MA. Removal of the basement membrane enhances corneal wound healing. Exp Eye Res. 2011; 93:927–36. [PubMed: 22067129]
22. Dickendesher TL, Duan Y, Giger RJ. Axon Regeneration. Comprehensive Developmental Neuroscience: Cellular Migration and Formation of Neuronal Connections. 2013:151–175.
23. Jung H, Yoon BC, Holt CE. Axonal mRNA localization and local protein synthesis in nervous system assembly, maintenance and repair. Nat Rev Neurosci. 2012; 13:308–24. [PubMed: 22498899]
24. Holt CE, Schuman EM. The central dogma decentralized: new perspectives on RNA function and local translation in neurons. Neuron. 2013; 80:648–57. [PubMed: 24183017]
25. Gaudet AD, Popovich PG, Ramer MS. Wallerian degeneration: gaining perspective on inflammatory events after peripheral nerve injury. J Neuroinflammation. 2011; 8:110. [PubMed: 21878126]
26. McCall MN, McMurray HR, Land H, Almudevar A. On non-detects in qPCR data. Bioinformatics. 2014; 30:2310–6. [PubMed: 24764462]
27. Hattori T, et al. Characterization of Langerin-expressing dendritic cell subsets in the normal cornea. Invest Ophthalmol Vis Sci. 2011; 52:4598–604. [PubMed: 21482644]
28. Reichard M, Hovakimyan M, Guthoff RF, Stachs O. In vivo visualisation of murine corneal nerve fibre regeneration in response to ciliary neurotrophic factor. Exp Eye Res. 2014; 120:20–7. [PubMed: 24412420]
29. Himanen JP, Nikolov DB. Eph signaling: a structural view. Trends Neurosci. 2003; 26:46–51. [PubMed: 12495863]
30. Rogakou EP, Nieves-Neira W, Boon C, Pommier Y, Bonner WM. Initiation of DNA fragmentation during apoptosis induces phosphorylation of H2AX histone at serine 139. J Biol Chem. 2000; 275:9390–5. [PubMed: 10734083]
31. Perez White BE, Getsios S. Eph receptor and ephrin function in breast, gut, and skin epithelia. Cell Adh Migr. 2014; 8:327–38. [PubMed: 25482622]
32. Hamrah P, et al. Unilateral herpes zoster ophthalmicus results in bilateral corneal nerve alteration: an in vivo confocal microscopy study. Ophthalmology. 2013; 120:40–7. [PubMed: 22999636]
33. Chao C, Golebiowski B, Stapleton F. The role of corneal innervation in LASIK-induced neuropathic dry eye. Ocul Surf. 2014; 12:32–45. [PubMed: 24439045]
34. Baratz KH, et al. Effects of glaucoma medications on corneal endothelium, keratocytes, and subbasal nerves among participants in the ocular hypertension treatment study. Cornea. 2006; 25:1046–52. [PubMed: 17133051]
35. Finci LI, et al. The crystal structure of netrin-1 in complex with DCC reveals the bifunctionality of netrin-1 as a guidance cue. Neuron. 2014; 83:839–49. [PubMed: 25123307]
36. Patel SV, Erie JC, McLaren JW, Bourne WM. Keratocyte and subbasal nerve density after penetrating keratoplasty. Trans Am Ophthalmol Soc. 2007; 105:180–9. discussion 189–90. [PubMed: 18427608]
37. Sacchetti M, Lambiase A. Diagnosis and management of neurotrophic keratitis. Clin Ophthalmol. 2014; 8:571–9. [PubMed: 24672223]
38. Labbe A, et al. The relationship between subbasal nerve morphology and corneal sensation in ocular surface disease. Invest Ophthalmol Vis Sci. 2012; 53:4926–31. [PubMed: 22695962]
39. Mehlen P, Delloye-Bourgeois C, Chedotal A. Novel roles for Slits and netrins: axon guidance cues as anticancer targets? Nat Rev Cancer. 2011; 11:188–97. [PubMed: 21326323]
40. Myers JP, Santiago-Medina M, Gomez TM. Regulation of axonal outgrowth and pathfinding by integrin-ECM interactions. Dev Neurobiol. 2011; 71:901–23. [PubMed: 21714101]

41. Erturk A, Hellal F, Enes J, Bradke F. Disorganized microtubules underlie the formation of retraction bulbs and the failure of axonal regeneration. J Neurosci. 2007; 27:9169–80. [PubMed: 17715353]

42. Han Y, et al. Netrin-1 simultaneously suppresses corneal inflammation and neovascularization. Invest Ophthalmol Vis Sci. 2012; 53:1285–95. [PubMed: 22323486]

43. Nikolopoulos SN, Giancotti FG. Netrin-integrin signaling in epithelial morphogenesis, axon guidance and vascular patterning. Cell Cycle. 2005; 4:e131–5. [PubMed: 15725728]

44. Walsh R, Blumenberg M. Specific and shared targets of ephrin A signaling in epidermal keratinocytes. J Biol Chem. 2011; 286:9419–28. [PubMed: 21193391]

45. Kojima T, Chang JH, Azar DT. Proangiogenic role of ephrinB1/EphB1 in basic fibroblast growth factor-induced corneal angiogenesis. Am J Pathol. 2007; 170:764–73. [PubMed: 17255342]

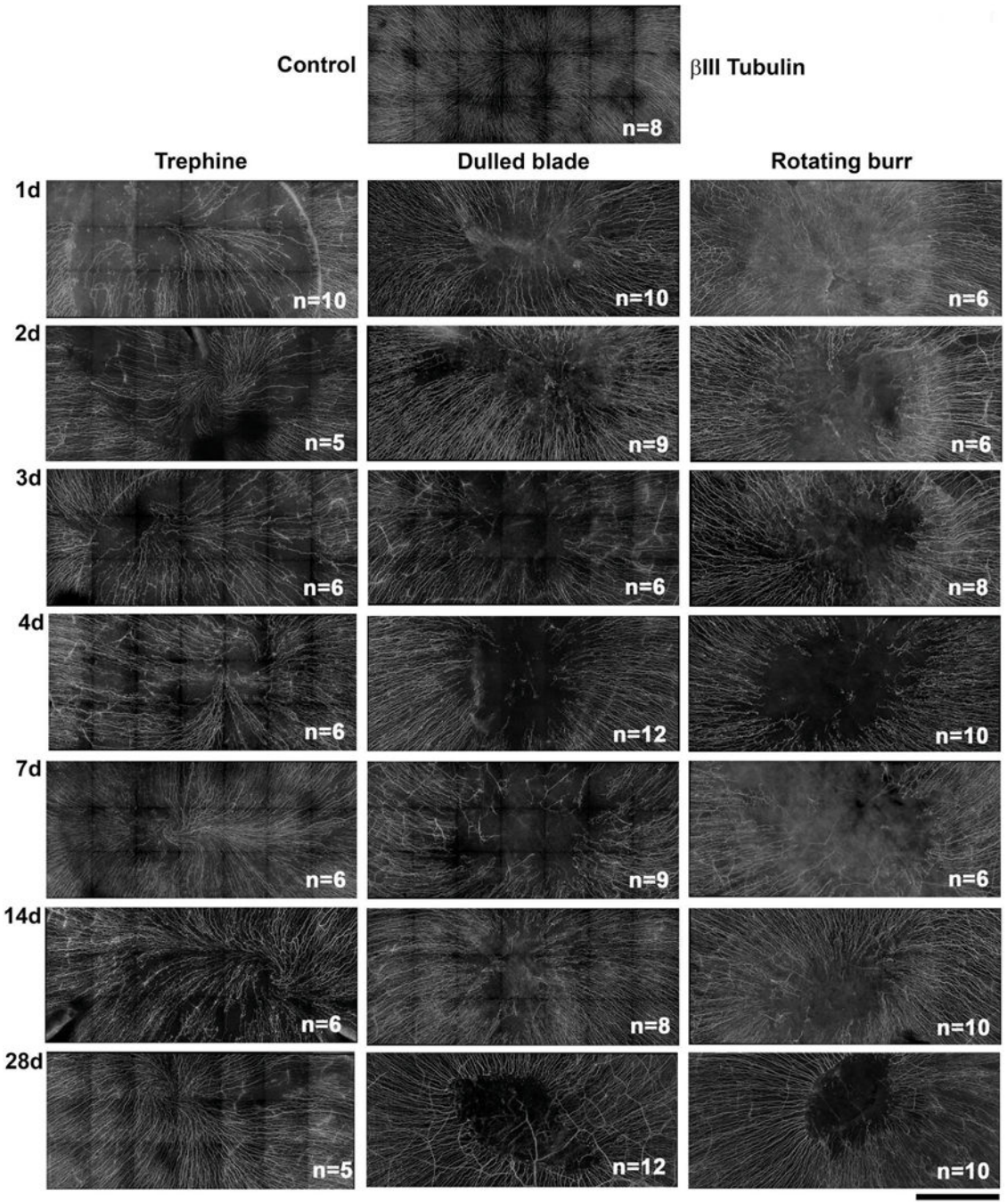

Figure 1. Subbasal axons fully reinnervate the cornea and reform the vortex over time after trephine wounding but not after dulled blade and rotating burr wounding

Representative stitched images of subbasal axons stained with βIII tubulin were taken by spinning disk confocal microscope to show the central 2 mm area of the mouse cornea encompassing the site demarcated by the 1.5 mm trephine in unwounded and corneas 1d, 2d, 3d, 4d, 7d, 14d, and 28d after wounding. The numbers of corneas used for quantification of reinnervation by Sholl analysis are indicated in the lower right corner of each image (Mag bar=500μm).

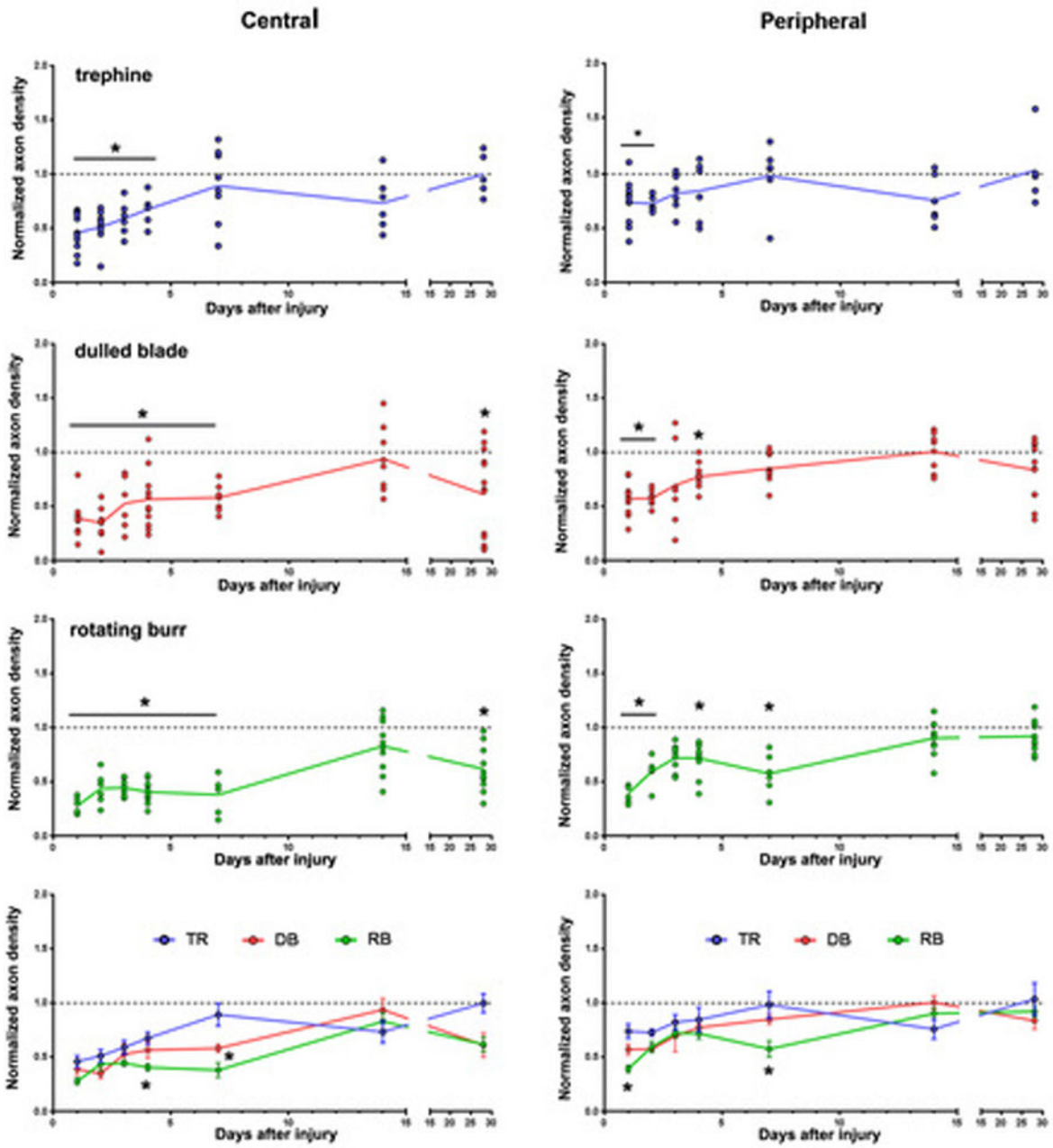

Figure 2. Fewer axons are present at the center of the cornea 28d after dulled blade and rotating burr wounds

The density of axons at the center and periphery of the cornea was determined by Sholl analysis. Data are expressed as the number of intersections present at the corneal center (left) and the periphery (right) at 1d, 2d, 3d, 4d, 7d, 14d, and 28d after wounding relative to the numbers of intersections in unwounded control corneas. Scatter plots with trendlines are presented for trephine (blue), dulled blade (red) and rotating burr (green) wounded corneas; filled circles indicate data from individual corneas. The parallel grey line at the value of 1.0 indicates axon density in control. Data are compared using one-way ANOVA and p values

less than 0.05 are considered significant. The graph at the bottom shows data from all three wound types plotted together to better visualize comparisons between wound types.

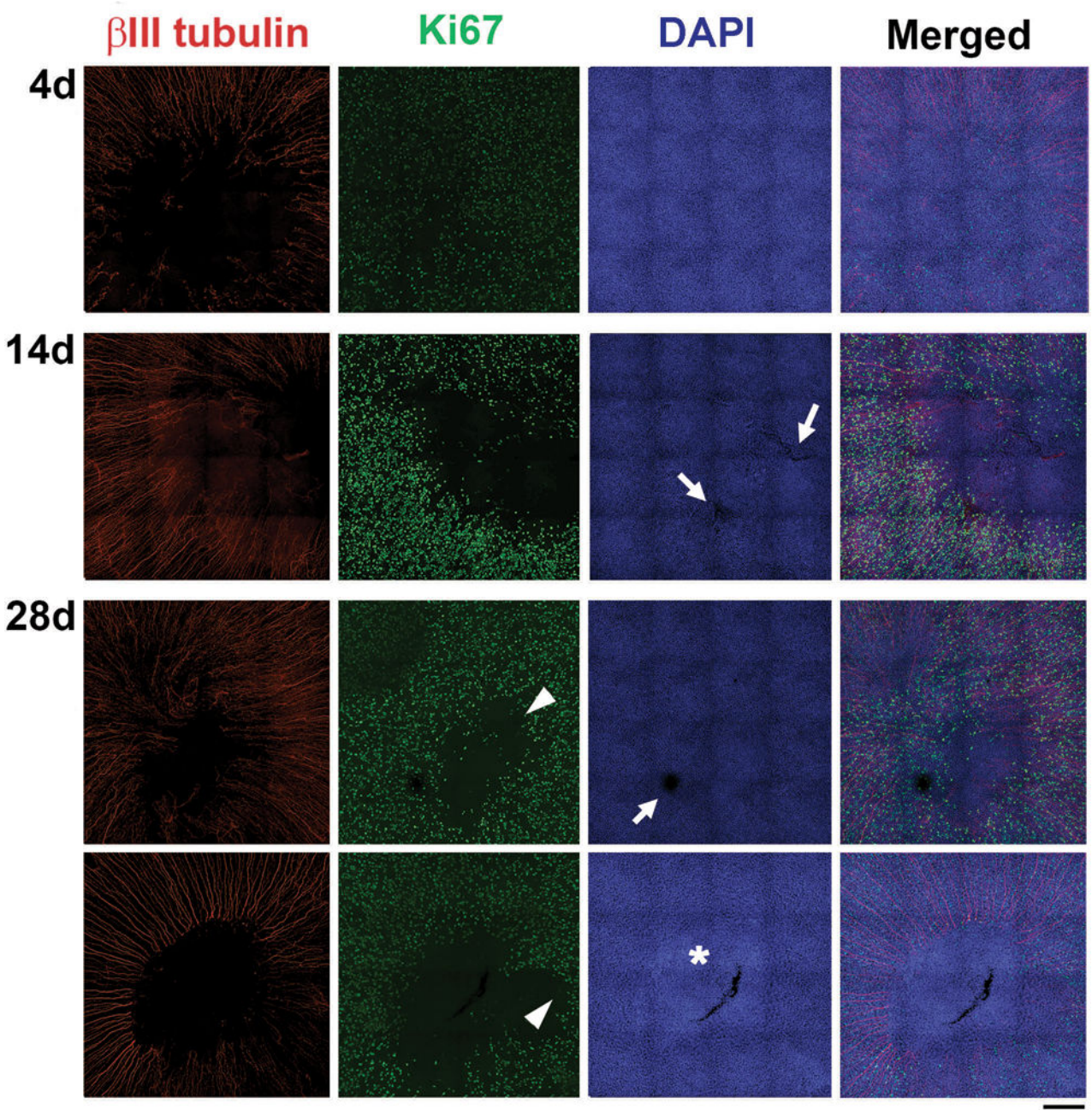

Figure 3. Disruption in the epithelial surface of rotating burr wounded corneas is evident at 14d after wounding

Representative stitched images of rotating burr wounded corneas at 4d, 14d, and 28d after wounding were stained with βIII tubulin, Ki67, and DAPI and imaged by spinning disk confocal microscope. White arrows indicate surface irregularities by 14d and 28d after wounding and white asterisks points out the thickening of the epithelium seen at 28d. The white arrowheads indicate reinnervated areas, which lack Ki67 (Mag bar=100μm).

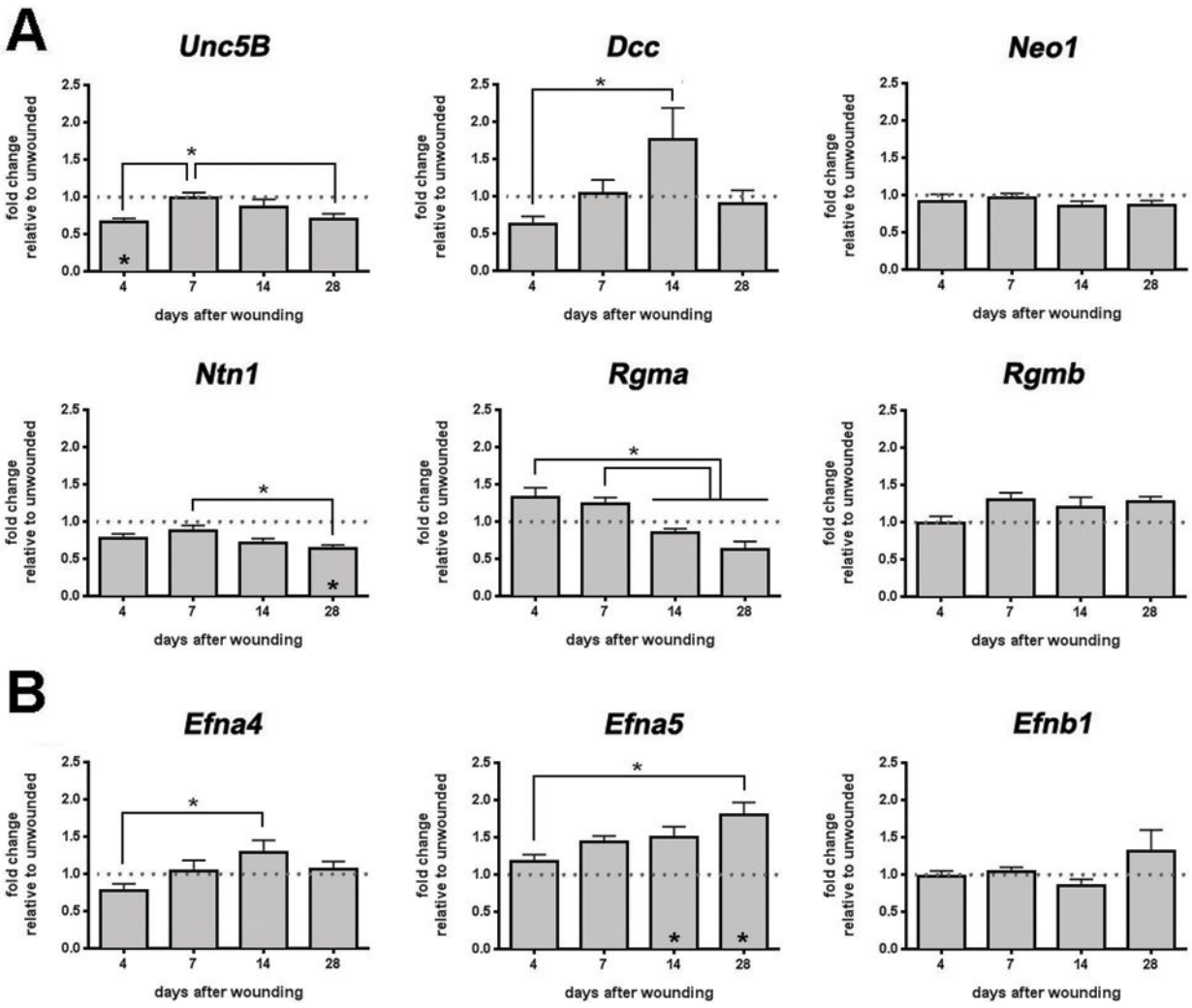

Figure 4. Expression of mRNA for *Ntn1 is* decreased and *Efna5* is increased in corneal buttons 28d after dulled blade wounding

QPCR analysis was performed on corneal buttons at 4d, 7d, 14d, and 28d after dulled blade wounding, using 22 primers as shown here and in the Supplemental Figure 2, and the expression level for each mRNA was normalized relative to GAPDH. The asterisks above the bars indicates significant differences between time points; asterisks within bars indicate significant differences relative to control. **A.** *Unc5b* is transiently but significantly decreased at 4d. While Dcc increased significantly between 4 and 14 days, the changes were not significant relative to control. *Ntn1* is reduced significantly at 28d after wounding relative to both control and to day 7. **B.** *Efna5* is increased at 14d and 28d after wounding as compared to control and at 28 days relative to 4 days.

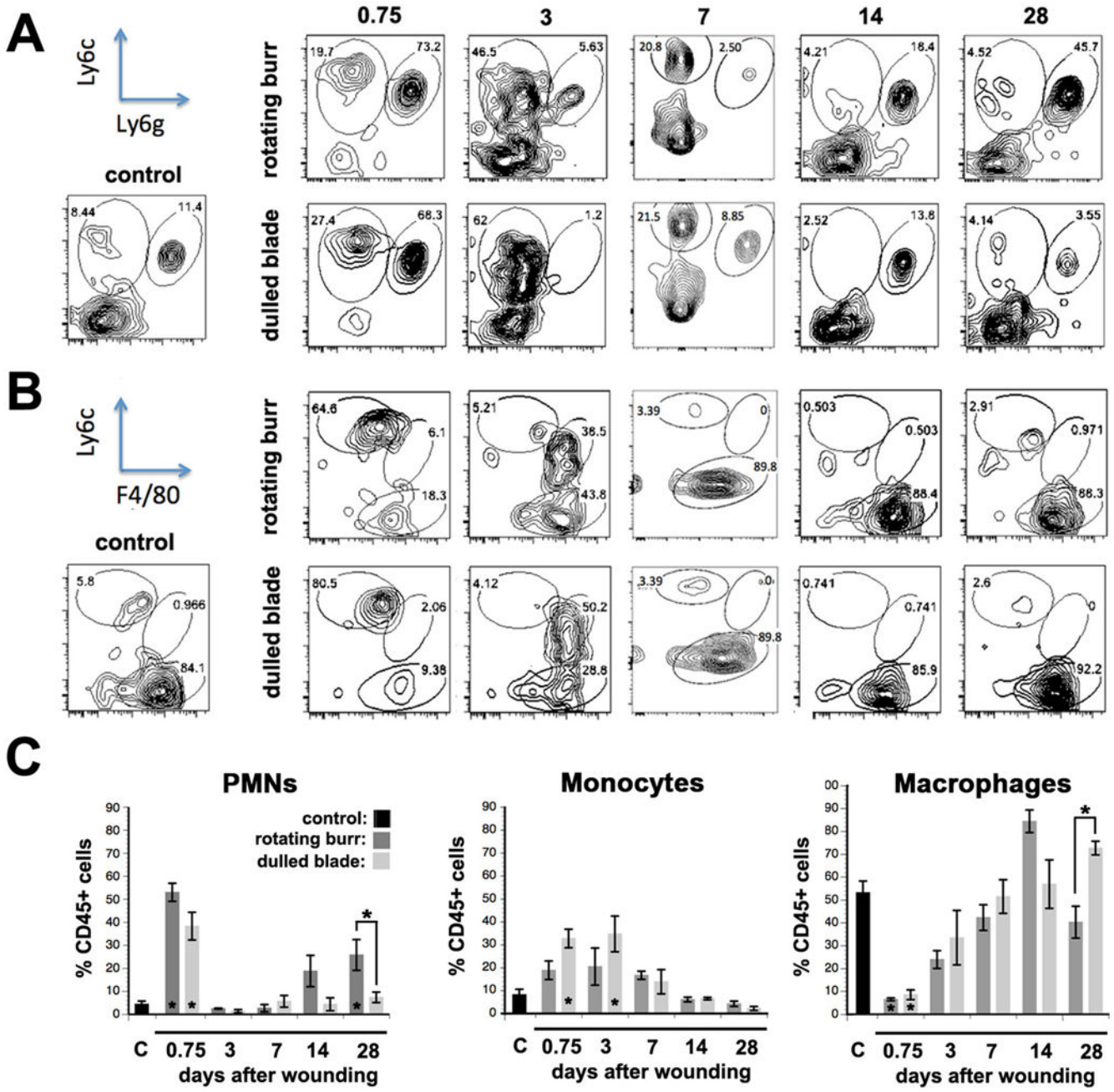

Figure 5. Flow cytometry shows that differences in leukocyte recruitment are seen after dulled blade and rotating burr wounds

A. Flow cytometric characterization of inflammatory cell populations in control, rotating burr, and dulled blade wounded corneas was performed at 0.75d (18 hours), 3d, 7d, 14d, and 28d after wounding. Four corneas were used per time point tested and the numbers of independent samples assayed was 4 for each wound type and time point. Representative flow cytometric data show PMNs (Ly6c+Ly6g-) and monocyte (Ly6c+Ly6g+) populations after gating for CD45+ cells. **B.** Leukocytes were also assessed for their expression of Ly6C and F4/80 after gating for CD45+CD11b+Ly6C- cells to determine whether there were

differences in maturation of monocytes into macrophages after both types of wounding. **C.** The means +/− SEMs of the percentages of CD45+ cells that are PMNs, monocytes, or macrophages were determined. Asterisks above bars indicate significant differences (p values less than 0.05 by one way ANOVA) between the means of rotating burr and dulled blade. Asterisks on bars indicate significant differences compared to unwounded control.

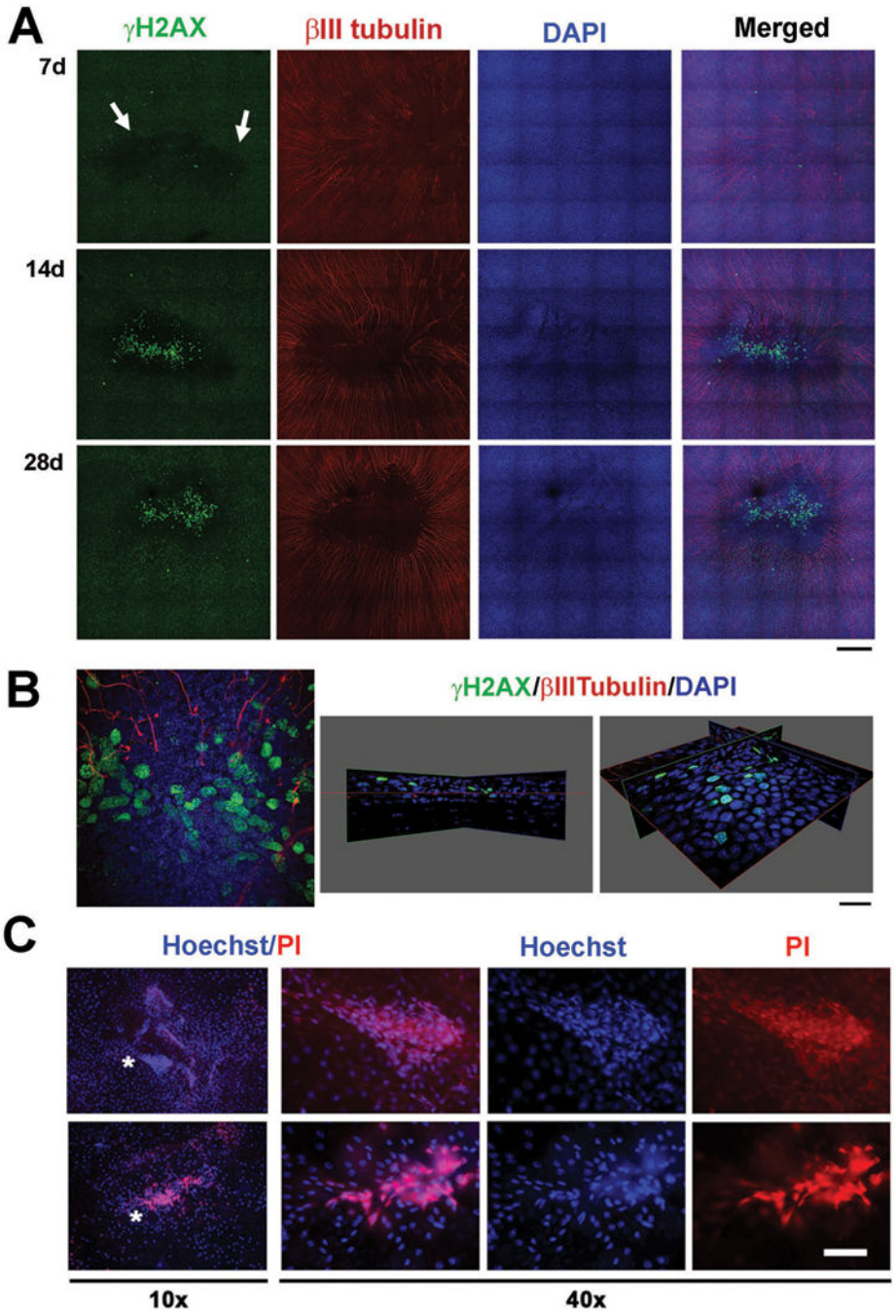

Figure 6. Apoptotic and dead cells develop on the epithelium after corneal wounding

A. To determine when cells at the corneal center begin to undergo apoptosis, dulled blade wounded corneas were stained with γH2AX, βIII tubulin, and DAPI at 7d, 14d, and 28d after wounding. White arrow indicates patches of cells expressing reduced levels of γH2AX (γH2AXlo) at 7d after wounding. These sites remain 14d and 28d after wounding corresponding to sites lacking nerves. Arrowheads show cells expressing high levels of γH2AX suggestive that they are undergoing apoptosis at 14d and 28d after wounding (Mag bar=100μm). **B.** The 14 day dulled blade wounded cornea shown in **A.** was subjected to high

resolution 3D confocal imaging. On the left is the en face view at the center of the cornea after wounding. On the right are two different 3D views tilted at different angles to show that while most of the γH2AX bright cells are in the basal cell layer, some cells are also seen in the suprabasal cell layers. (Mag bar=10μm). **C.** To determine whether apoptotic cells undergo apoptosis and/or die, unfixed corneas obtained immediately after sacrifice of mice 28d after dulled blade wounding were stained with Hoechst and PI and images were taken at 10× (left) and 40× (right) with a fluorescent microscope. Hoechst+ apoptotic and PI+ dead cells are present within the corneal epithelium adjacent and within sites that appear to be erosions. Asterisks show the areas in the 10× images where the 40× images were obtained.